Chapter 7
Microdischarges in High Vacuum

The ion microscope generally equips the electrostatic lens system using high voltage electrodes, which often causes the problem concerning microdischarges in vacuum. Also, high-voltage transmission electron microscopes may meet problems concerning microdischarges in the electron beam acceleration tubes. When microdischarge, even a very small one, occurs in observing electron-microscope images, it causes inferior image quality.

Two kinds of microdischarge may occur, microdischarge over an insulator surface and one between high-voltage electrodes.

Keywords

Triple junction (cathode side): Junction of cathode, insulator, and vacuum.
Anode-initiation model: Anode-initiated microparticles approach the cathode, which becomes a trigger to initiate microdischarge.
Total voltage effect: In a multi-electrode high-voltage system, the breakdown voltage is limited by the total voltage applied between the top electrode and the bottom electrode rather than by the electric field in each electrode gap.
Ion-exchange process: Microdischarge occurs due to the regenerative exchange of positive ions and negative ions between the top electrode and the bottom electrode.
Conditioning: Aging of high-voltage system with application of a high voltage. After conditioning, a higher voltage could be applied without accompanying microdischarge.
AGC (Argon-glow conditioning): An argon glow discharge treatment for electrodes and insulators for aging. Typical conditions: 350 Vac, 180 mA, 5 min in about 10 Pa of argon.
HVC (high-voltage conditioning): A voltage higher than the rated voltage is applied in high vacuum for aging.

7A Microdischarges over Insulator Surfaces

Factors

Gleichauf (1951) [7A-1] presented an article, "Electrical breakdown over insulators in high vacuum."

Abstract [7A-1]: The breakdown voltage of vacuum gaps depends on the electrode material, but when the gap is bridged by an insulator it is independent of the electrode material and varies with the kind of insulator. Some indication is found that the breakdown voltage increases with increasing surface resistivity of the insulator, but no apparent correlation is found between breakdown voltage and dielectric constant, density, or vapor pressure. It is found that a roughening of the intervening surface of the insulator in the region adjacent to the cathode increases the breakdown voltage. For electrode separations of 1 mm or greater the breakdown voltage does not increase linearly with the length of the insulator. (The relationship $V_B \propto \sqrt{L}$ has been found, where L is the length of insulator and V_B is the breakdown voltage.) Experiments were made in which one of the electrodes was separated from the insulator. It seems that the critical gradient at breakdown in the vacuum space between the cathode and the insulator, calculated for the case of plane electrodes from the ratio of dielectric constants, is not as large as would be required in gaps without insulators. These gradients are almost the same for copper as for stainless steel electrodes. The breakdown voltage over an insulator is raised when the edge of the insulator close to either electrode is rounded. When a layer of glass, thin compared with the separation of electrodes, is fused to the cathode, breakdowns occur at lower voltages than for an identical vacuum gap.

Pillai and Hackam (1985) [7A-2] measured the surface flashover of Teflon, Plexiglas, quartz, Pyrex glass, Macor glass-ceramic, and sapphire solid insulators in vacuum ($\sim 10^{-8}$ Torr, $\sim 10^{-6}$ Pa) and in atmospheric air using dc, ac (60 Hz), and $1.2/50-\mu$sec lightning impulse voltages.

Abstract [7A-2]: The dependence of the flashover voltage on the following parameters is investigated: (1) spacer material, (2) diameter of the spacer, (3) spacer length, (4) number of spacers stacked in series, (5) air pressure in the range 10^{-6} to 10^5 Pa, (6) electrode material, (7) spark conditioning, and (8) the external resistance in series with the gap. At a fixed insulator length the flashover voltage decreases with increasing spacer diameter. The withstand voltage of spacers stacked in series increases with increasing the number of spacers. The dc flashover voltage of different insulating materials is theoretically calculated in vacuum as a function of the length of the insulator and compared with the experimentally obtained results. Good agreement is obtained.

Charging of Dielectric Surfaces

Tourreil and Srivastava (1973) [7A-3] presented an article, "Mechanism of surface charging of high-voltage insulators in vacuum.

Abstract [7A-3]: In vacuum, the surface of insulators becomes electrically charged when subjected to high-voltage stresses. The charging mechanism is described. A model simulating the charging shows that the surface charge densities are proportional to the applied voltage and depend on the secondary electron emission of the dielectric surface. It is also time dependent. Surface charges are shown to explain many results obtained in studies of insulator surface breakdown.

Sudarshan and Cross (1973) [7A-4] presented an article, "DC electric-field modifications produced by solid insulators bridging a uniform-field vacuum gap."

Abstract [7A-4]: The results of measurements of the electric field near the surface of stainless-steel electrodes in vacuum are described. It is found that the field is modified by a solid insulator bridging the inter-electrode gap. The extrapolated cathode field is enhanced sufficiently to equal the value considered necessary to initiate breakdown in a plane vacuum gap. The measured fields are greater than the applied field and consistent with the accumulation of positive surface charge on the solid insulator. Analysis of the data suggests that the surface charge results from bombardment of the surface by electrons emitted at the insulator-cathode junction.

The characteristics of junction-field vs. applied-field measured for alumina are presented in **Fig. 7A.1** [7A-4].

Anderson and Brainard (1980) [7A-5] presented an article, "Mechanism of pulsed surface flashover involving electron-stimulated desorption."

Surface Flashover Model [7A-5]

Secondary Emission Avalanche [7A-5]:
A magnified view of the insulator surface early in the pre-breakdown time delay is shown in **Fig. 7A.2**. The layers of avalanche electrons, neutrals, and positive ions are identified, and typical trajectories of each of these particles are indicated. Electrons drift toward the anode through repeated secondary emission events of unity yield, as if hopping across the insulator surface; neutrals drift away from the surface; and ions are accelerated away from the surface and toward the cathode.

Observation of Avalanche Current [7A-5]:
Measurements of the current of electrons arriving at the anode electrode at the edge of a 20 mm-long rectangular insulator (**Fig. 7A.3**) are consistent with the description of discharge development summarized above. Electrons passing through a 1.5 mm-diam hole in the anode electrode were collected by a shielded Faraday cup. A small needle on the cathode electrode initiated a region of surface charging in line with the hole in the anode electrode. Typical simultaneous cathode voltage and Faraday-cup current waveforms obtained from an alumina ceramic insulator are displayed in **Fig. 7A.4**. Results for polymethyl methacrylate (Plexiglas) are similar.

The waveforms in **Fig. 7A.4** indicate that after an initial burst of current corresponding to a few tenths of an ampere per mm surface current, a smaller steady current persisted until it grew rapidly immediately prior to the collapse of insulator impedance. As the secondary emission avalanche propagated across the insulator, some of the emitted electrons apparently escaped the avalanche and were accelerated to the anode to be detected as the initial burst of current (which may be seen in **Fig. 7A.4** as a 1.5 ns-wide hump in the current waveforms occurring soon after the cathode voltage attains its maximum value). The steady current observed during the latent period prior to breakdown is roughly equal to the predicted current due to the slow drift of avalanche electrons toward the anode.

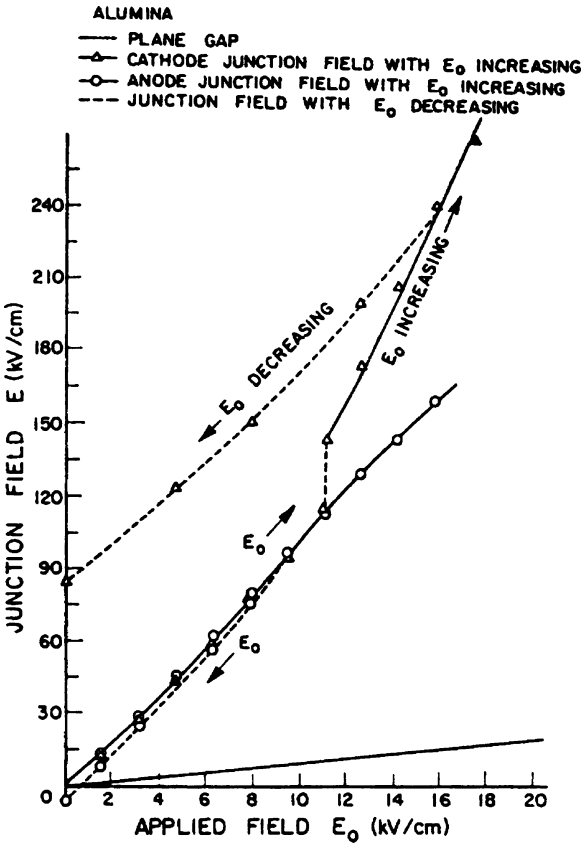

Fig. 7A.1 Junction field vs. applied field for alumina. Insulator making flat contact with electrodes (Sudarshan and Cross, 1973) [7A-4]

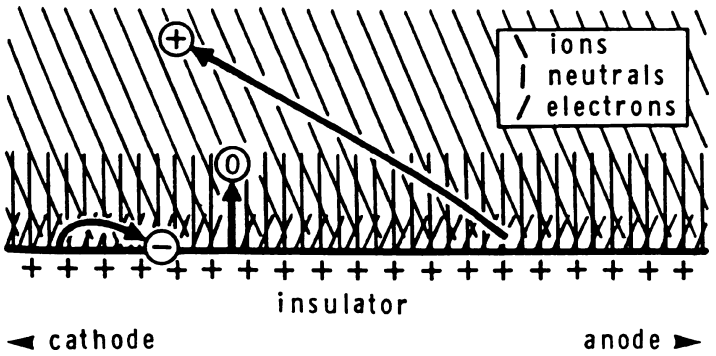

Fig. 7A.2 Layers and avalanche electrons, neutrals, and positive ions early in the prebreakdown delay time. Typical trajectories of each of these particles are indicated (Anderson and Brainard, 1980) [7A-5]

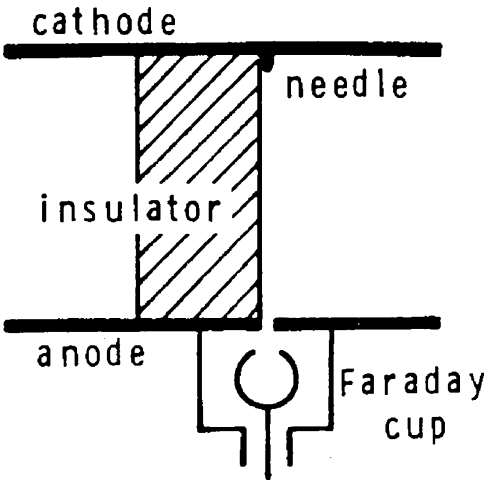

Fig. 7A.3 Arrangement for measuring the prebreakdown current. The hole in the anode electrode is aligned with a small needle attached to the cathode electrode and in contact with the insulator. The anode is at ground potential (Anderson and Brainard, 1980) [7A-5]

Pillai and Hackam (1982) [7A-6] presented an article, "Surface flashover of solid dielectric in vacuum."

Analysis of the Charging Mechanism [7A-6]
The secondary electron emission rate δ from an insulator surface initially increases with increasing impinging energy of the electrons until it reaches saturation and starts to decrease at high energy. There are two energies at which $\delta = 1$ [3].

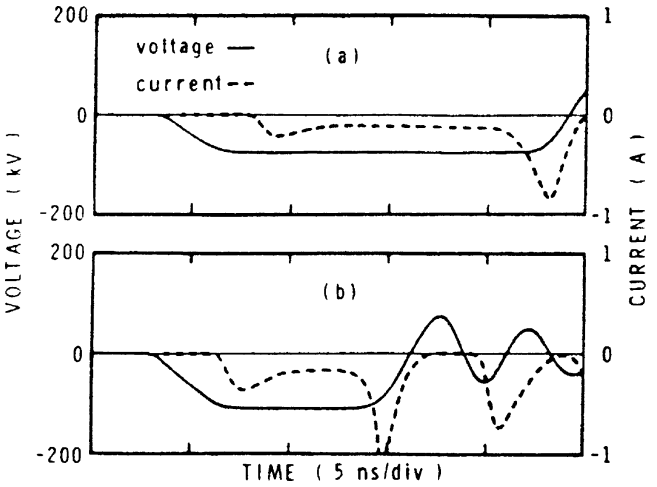

Fig. 7A.4 Simultaneous cathode voltage and Faraday-cup current waveforms, measured as in **Fig. 7A.3** (alumina ceramic insulator 20 mm long). Collapse of impedance at breakdown is evidenced by the onset of inductive-capacitive ringing in the cathode voltage. The applied voltage was 46% larger in (**b**) than in (**a**), which reduced the prebreakdown time delay by a factor of approximately 2 (Anderson and Brainard, 1980) [7A-5]

In the initial stage of charging, all the electrons striking the insulator's surface are emitted from the triple junction. The impinging energy is that gained from the inter-electrode field, neglecting the energy of emission from the cathode [2]. The region on the insulator surface struck by electrons yielding $\delta > 1$ becomes positively charged. Near the anode, the surface becomes at first slightly negatively charged. When the surface-charge density of the positively charged region becomes sufficiently high, many of the secondary electrons emitted from the insulator surface will be attracted back onto the surface. The trajectory range of the electrons emitted from the insulator's surface will decrease as the surface-charge density increases. The energy at impact will therefore decrease. It will do so until the impact energy becomes equal to that corresponding to $\delta = 1$ which is the stable operating point and any deviation from it is self-correcting. This also corresponds to the electric field which is inclined at the critical angle with respect to the insulator surface [1, 2].

An electron emitted from the surface with energy A_0 and having a direction normal to the insulator surface reaches height x

$$x = (A_0 / eE_\perp), \tag{7A.1}$$

where x is cm, A_0 in eV and $E_\perp$ (in V/cm) is the field normal to the surface of the insulator resulting from the surface charge density.

The range of the trajectory is

$$y = (4A_0 E_{//} / eE_\perp^2), \tag{7A.2}$$

where y is in cm and $E_{//}$ (in V/cm) is the field parallel to the surface of the insulator and equal to the average applied field in the case of a solid cylindrical insulator. $E_{//} = V/l$, where V is the applied voltage between the electrodes and l the gap spacing. Taking into account the cosine-law distribution in the direction of emission, the average value of impact energy A_i becomes [1]

$$A_i = A_0 \left[1 + 2(E_{//}/E_\perp)^2\right]. \tag{7A.3}$$

When the steady state of charging is reached at unity yield, the impinging energy is A_1. It should be noted that the stability of the surface charge corresponding to the lower of the two energies A_1, at which the emission yield is unity, is sufficient to be considered [4]. The relationship between the field $E_{//}$ and the field $E_\perp$ is [5]

$$E_{//} = E_\perp \sqrt{\frac{1}{2}\left[(A_1/A_0) - 1\right]}. \tag{7A.4}$$

The height of the trajectory is very small, a few micrometers, compared to the radius of curvature of the surface of practical insulators, and therefore can be considered as a plane as far as the trajectory of the electron is concerned. The field produced by the positive charge in the plane geometry is

$$E_\perp = \sigma_+ / 2\varepsilon_0, \tag{7A.5}$$

where ε_0 is the permittivity of the free space (8.85×10^{-14} F/cm) and σ_+ is the charge density in C/cm^2.

The critical angle for which the surface charge is at an equilibrium is given by $\tan\theta$. θ is the angle between the electric field and the insulator surface. The value of $\tan\theta$ mainly depends on the impact energy A_1.

$$\tan\theta = (E_\perp / E_{//}) = \sqrt{2A_0/(A_1 - A_0)}. \tag{7A.6}$$

In general, the secondary-emission parameters A_0 and A_1 for solid insulators are a few eV and a few tens of eV, respectively. Using the data available on the secondary-electron emission yield from insulators [3], the value of θ obtained from Eq. (7A.6) is found to vary

from about 10°–35°. The expression for positive surface charge density σ_+ can be written in terms of the interelectrode field $E_{//}$

$$\sigma_+ = 2\varepsilon_0 E_{//} \tan\theta. \tag{7A.7}$$

The current carried by the secondary emission avalanche depends on the density of negative space charge σ_- and the drift velocity of electrons in the avalanche. The density of the electrons' space-charge in the emitted secondary electron avalanche cannot exceed the surface charge σ_+ in magnitude without causing electrons to be repelled from the insulator. When the electrons drift towards the anode, the value of σ_- diminishes, but at the same time, the positive surface charge at the insulator-cathode junction enhances the field at the cathode triple junction. The increased field emission maintains σ_- equal to σ_+. Hence in our analysis, it is assumed that σ_- is equal to σ_+. The surface current carried by the secondary emission avalanche per centimeters can be written as

$$I_{//} = \sigma_- v_e, \tag{7A.8}$$

where $I_{//}$ is the current per unit length of the insulator surface (A/cm). The average velocity v_e is used as an approximation for the drift velocity.

$$v_e = \sqrt{2A_1 \times 10^4 / m_e},\ (\text{cm/s}) \tag{7A.9}$$

where m_e and e are the electron mass and charge, respectively. A_1 is expressed in joule.

From the above relation, the average velocity of an electron in the avalanche having an energy A_1 eV is

$$v_e = 5.94 \times 10^7 . \sqrt{A_1} \tag{7A.10}$$

The surface current expression becomes

$$I_{//} = \sigma_- \times 5.94 \times 10^7 \times \sqrt{A_1}.\ (\text{A/cm}) \tag{7A.11}$$

The electrons return to the insulator after traveling an average distance of $s = A_1 / E_{//}$. The value of s is of the order of 10^{-4}–10^{-3} cm, when σ_+ is at a saturated steady state. The current density perpendicular to the insulator surface can be obtained as

$$J_\perp = (\sigma_- v_e E_{//} / A_1).\ (\text{A/cm}^2) \tag{7A.12}$$

The desorption rate from the insulator surface depends on $J_\perp$.

Electron-Impact Gas Desorption and Discharge Formation [7A-6]

When electrons impinge on the surface of a solid insulator, the particles released, depending on the electrons' energy, include neutral molecules, atoms, excited neutrals, and positive and negative ions. The ratio of neutrals evolved is very much higher than other particles. In most cases, the electron-impact desorption cross-sections are smaller than the corresponding ionization cross-section in the gas phase. Electron impact cross-sections vary with electron energy in a similar fashion to gas-phase ionization cross-sections. The average desorption cross-section is assumed to be $10^{-16}\,\text{cm}^2$ [6], as the major components of the desorbed gases are carbon monoxide and hydrogen.

The electron-stimulated desorption (ESD) efficiency can be found from experiments on pre-breakdown currents by measuring the outgassing rates of gases [6, 7]. It is assumed that the pre-breakdown current is due to secondary-emitted electrons hopping across the surface of a fully charged insulator. For CO, H_2, N_2, H_2O, and other molecules which are known to be adhered to the surface, the number of molecule per square centimeter on the surface of the dielectric may be taken as the order 10^{16}–$10^{17}/\text{cm}^2$ [8, 9]. In order to estimate the desorption probability, the results found in a study of the gas evolution from insulators

subjected to an electric field in the direction parallel to the surface are considered [7]. The rate of gas evolution depends on the insulating material as well as the desorption probability. A value of outgassing rate of the order of $2–5 \times 10^{-7}$ Torr · L/s for different insulating materials (Plexiglass, Teflon, vinyl, ceramics) has been reported [7]. The desorption probability corresponding to this outgassing rate is in the range 5–15 molecules per impinging electron calculated from pre-breakdown currents of $2–6 \times 10^{-7}$ A observed in our (Pillai and Hackam) experiments. A desorption probability of a few molecules per electron is consistent with the product of an electron-stimulated desorption cross-section of a small multiple of $10^{-16}\,\mathrm{cm}^2$ [6, 10] and the number of molecules per square centimeter on the surface of 10^{16}–10^{17} [8, 9].

The rate of electron-impact gas desorption J_d depends on the electron-current density $J_\perp$ $(\mathrm{A/cm}^2)$, the desorption cross-section Q_d (cm^2) and the surface-charge density σ_d $(\mathrm{molecules/cm}^2)$. The expression for J_d is

$$J_d = (\sigma_d Q_d J_\perp / e)(\mathrm{molecules} \cdot \mathrm{cm}^{-2} \cdot \mathrm{s}^{-1}). \tag{7A.13}$$

In general the desorbed particle rate is written as

$$J_d = (\gamma J_\perp / e), \tag{7A.14}$$

where γ is the desorption probability equal to $\sigma_d Q_d$ molecules/electron.

The electron stimulated desorption probability of gases from a clean and well-outgassed insulator surface can be found by observing the pressure changes in the system housing it during electron bombardment of the sample [10]. The variation in the desorption rate for a particular insulator depends among other things on the sample temperature, the electron-impact energy and the electron-current density. The main components of the desorbed gases are hydrogen, nitrogen, carbon monoxide, and water vapor. The relative amount of these gases present depends on the structure, composition, and history of the insulator. The desorbed gases from materials like Teflon (polytetrafluoroethylene), Plexiglass (polymethyl methacrylate), ceramics, alumina (Al_2O_3) contain a higher percentage of hydrogen and water vapor particularly in the case of an unbaked vacuum system. In a well-baked system the gases normally consist of at least 30–50% CO. In order to find the density of desorbed gas, the velocity v_0 at which a desorbed neutral leaves the insulator surface must be known. However, only a few data are available on the value of v_0. The average velocity of the gas molecules may be assumed of the order of $1.5–2.0 \times 10^5$ cm/s [3, 11, 12] The density of the desorbed molecules N_d can be estimated from the value of v_0 and the gas-desorption rate

$$N_d = (\gamma J_\perp / e v_0)\ (\mathrm{molecules/cm}^3). \tag{7A.15}$$

The amount of the desorbed gas M per square centimeter from the insulator surface due to a pre-discharge field current is given by the product of N_d and the length of the insulator, l

$$M = (\gamma J_\perp / e v_0) l. \tag{7A.16}$$

Flashover Breakdown Criteria [7A-6]

The electrical field is enhanced at the cathode end of the insulator due to the effect of positive-charge accumulation, and consequently, the electron-emission current from the cathode increases. Increasing the applied electric field leads to a rise in the field-emission current, and consequently, the amount of desorbed gas increases. The ionization rate increases rapidly with increasing of the desorbed gas. When the pre-breakdown current is low, the gas desorption is also low. In this case, the condition for a self-sustained discharge can only be satisfied at a very high field. There is obviously some critical current I_{cr} and a corresponding critical desorbed amount of gas density M_{cr} at which the electron density required for breakdown is reached [13].

The breakdown field can be calculated from the value of M_{cr} corresponding to I_{cr}.

From Eqs. (7A.5), (7A.6), (7A.12), (7A.16) and assuming $M = M_{cr}$, the critical value at the onset of the surface flashover, the expression for the field $E_{//}$ required to cause flashover can be written as

$$E_{//} = \sqrt{\frac{M_{cr} A_1 v_0 e}{2\varepsilon_0 l \gamma v_e \tan\theta}}. \text{ (V/cm)} \tag{7A.17}$$

Equation (7A.17) indicates the dependence of $E_{//}$ on the secondary-electron impact energy, desorption probability and length of the insulator. It also gives a correct description of the decrease in the dielectric strength of the surface with increasing insulator length.

The breakdown voltage can also be calculated by using Eq. (7A.17). The breakdown voltage is almost independent of the electrode material and strongly dependent on the insulator material [7, 14]. The breakdown voltage V_B is

$$V_B = E_{//} l = \sqrt{\frac{M_{cr} A_1 v_0 e l}{2\varepsilon_0 \gamma v_e \tan\theta}}. \text{ (V)} \tag{7A.18}$$

Equation (7A.18) shows that the flashover voltage across a solid insulator held between two planar parallel electrodes increases in a nonlinear form with increasing length of the insulator. The reported results of [14, 15, 16, 17, 18] are plotted in **Fig. 7A.5** for various insulating materials where it can be seen that a dependence of the flashover voltage on length of the insulator to a power law of $\sqrt{l}$ is suggested. The predicted dependence of the flashover voltage given by Eq. (7A.18) on insulator length l is close to that observed experimentally (**Fig. 7A.5**).

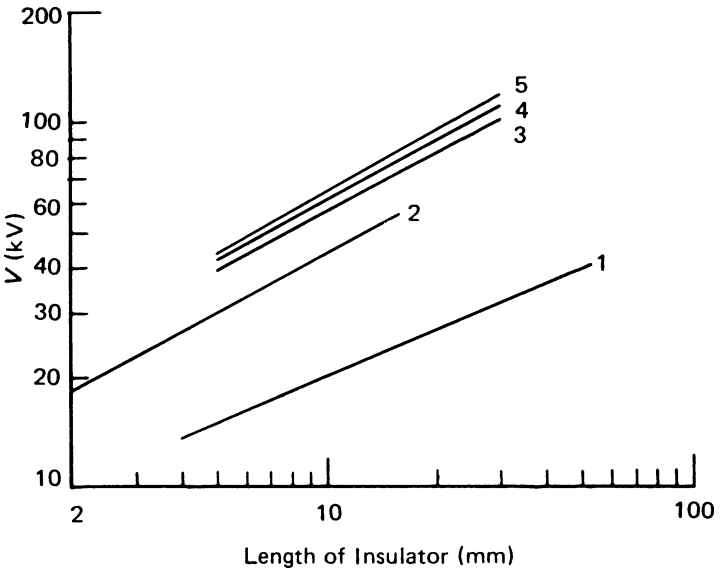

Fig. 7A.5 Flashover voltage as a function of insulator length for different materials. (1) Pyrex [17], (2) Alumina ceramic [18], (3) Polyethylene [16], (4) Teflon [16], (5) Plexiglass [16] (Pillai and Hackam, 1982) [7A-6]

References

1. H. Boersch, H. Hamisch, and W. Ehrlich, *Z. Angew Phys.* **15**, 518 (1963).
2. C. H. De Tourreil and K. D. Srivastava, *IEEE Trans. Elect. Insul.* **8**, 17 (1973).
3. S. C. Brown, *Basic Data of Plasma Physics* (MIT, Cambridge, 1959).
4. R. A. Anderson and J. B. Brainard, *J. Appl. Phys.* **51**, 1414 (1980).
5. J. P. Brainard and D. Jensen, *J. Appl. Phys.* **45**, 3260 (1974).
6. P. A. Redhead, J. P. Hobson, and E. V. Kornelson, *The Physical Basis of Ultrahigh Vacuum* (Chapman and Hall, London, 1968).
7. A. A. Avdienko and A. V. Kiselev, *Sov. Phys. Tech. Phys*. **12**, 381 (1967).
8. S. P. Bugaev, A. M. Iskoldskii, and G. A. Mesyats, *Sov. Phys. Tech. Phys.* **12**, 1358 (1968).
9. S. Dushman and J. M. Lafferty, *Scientific Foundations of Vacuum Technique* (Wiley, New York, 1962).
10. M. J. Drinkwine and D. Lichtman, *Prog. Surf. Sci*. **8**, 123 (1977).
11. J. H. Leck and B. P. Stimpson, *J. Vac. Sci. Technol.* **9**, 293 (1972).
12. A. A. Avidenko and M. D. Malev, *Sov. Phys. Tech. Phys.* **24**, 581 (1979).
13. H. Raether, *Electron Avalanches and Breakdown in Gases* (Butterworth, London,1964).
14. R. Hawley, *Vacuum* **18**, 383 (1968).
15. Hackam, IEE invited review for colloqium "*Electrical Phenomena on Insulating Surfaces in Gases and in Vacuum*," IEE Digest No. 26 (1975).
16. S. Grzybowski and E. Kuffel, *IEEE Trans. Power Appar. Syst*. **99**, 1788 (1980).
17. P. Gleichauf, *J. Appl. Phys*. **22**, 766 (1951).
18. O. I. Kondratov, *Proceedings of the 5th International Symposium on Discharge and Electrical Insulation in Vacuum*, Poznan, Poland, 1972, p. 289.

Cross and Sudarshan (1974) [7A-7] experimentally investigated the effect of a cuprous oxide coating upon the surface flashover of high-density alumina in vacuum.

Abstract [7A-7]: It is shown that such coatings improve the impulse strength of the system and eliminate the conditioning effect observed in the case of uncoated specimens at dc and 60 Hz voltages. An explanation of the observed behavior is given in terms of a surface charging model. It is postulated that the improvement in the insulation by the coatings is due to a reduction in the secondary electron emission yield.

Sudarshan and Cross (1976) [7A-8] experimentally investigated the effect of chromium oxide coatings upon the surface flashover of high-density alumina in vacuum.

Abstract [7A-8]: It is shown that such coatings improve the withstand voltage for dc and 60 Hz, and impulse voltages by significant amounts. The coatings are simply applied, effective, and durable. It is postulated that the improvement in insulation is due to the elimination of positive surface charging by the use of a coating with a secondary-electron emission coefficient less than unity for all incident electron energies.

Gas Molecules on Insulator Surfaces

Watanabe et al. (1987) [7A-9] experimentally examined microdischarges on an electron gun (**Fig. 7A.6**) operated at 100 kV, by concentrating the greatest interest on gas molecules on the insulator and electrode surfaces.

Experiment [7A-9]
Microdischarge depends on the concentration of electric field in the gun chamber. Equipotentials around and on the electron gun, simulated by the finite-element method, are presented in **Fig. 7A.6**. The electric field is relatively high near the top and side of the Wehnelt electrode.

The holes of the Wehnelt and anode electrodes through which an electron beam passes are about 0.4 mm and 6 mm in diameter, respectively. The surfaces of the electrodes and chamber walls (304 stainless steel) are mirror-polished. The insulator is a kind of porcelain whose surface has been treated to be glassy. The junction of metal and insulator is covered by a guard ring (304 stainless steel, mirror polished) in electrical and mechanical contact with the Wehnelt electrode.

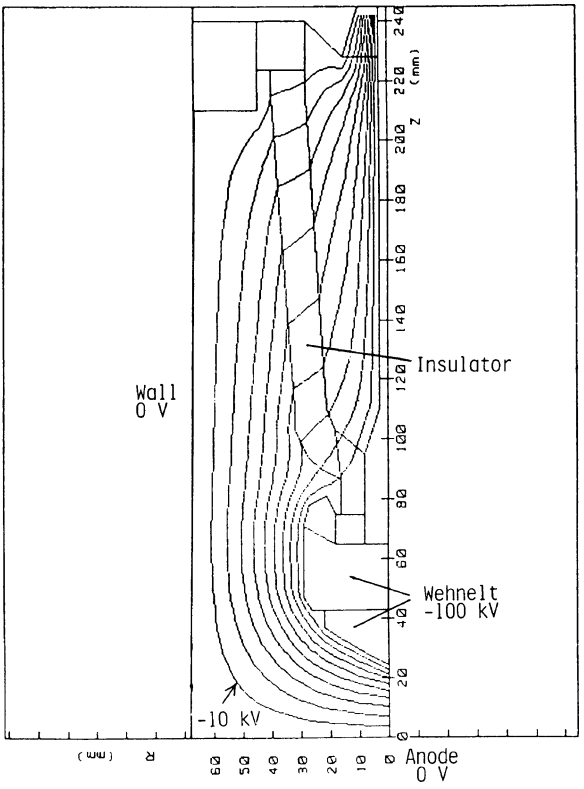

Fig. 7A.6 Equipotentials in a gun chamber with a 100 kV electron gun, which were simulated by the finite-element method (Watanabe et al., 1987) [7A-9]

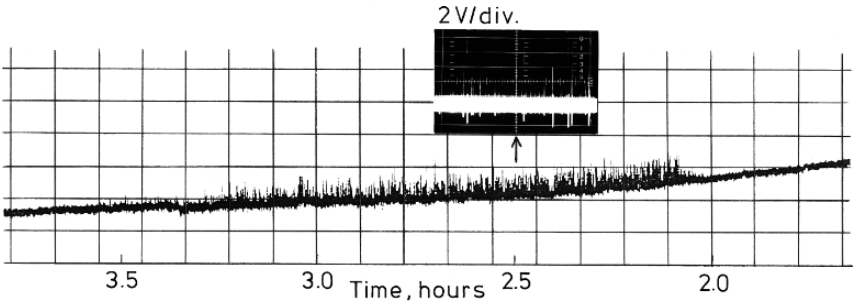

Fig. 7A.7 Microdischarges under about 10^{-4} Pa on "C-1" (1st day after cleaning) without AGC (Ar-glow conditioning) during an earlier period of the elapsed time. Microdischarges can be identified as voltage spikes on the chart line (Watanabe et al., 1987) [7A-9]

Experiments were conducted using a typical DP evacuation system. –100 kV is applied to the Wehnelt electrode with the anode electrode being kept at ground potential.

Microdischarges occurred most frequently on C-1 (1st day after CH_3CCl_3 cleaning) without AGC (Ar-glow conditioning), as presented in **Fig. 7A.7**, where microdischarges are identified as voltage spikes on an oscilloscope and on a recorder line. Microdischarges began to occur at about 2 h and occurred very frequently in the period from 2 h to 3.5 h.

We considered that microdischarges depending on the elapsed time must be related to the outgassing of the electron gun heated by the tungsten-filament emitter. During electron-beam extraction, the heat (about 10 W) from the filament emitter must be gradually raising the temperature of the insulator, resulting in increased outgassing from the insulator.

The outgassing from the insulator was examined by measuring pressure-increases caused by the lighted filament emitter and by analyzing evolved gases, in an SIP (sputter ion pump) evacuation system presented in **Fig. 7A.8**. Pressure-changes under various conditions in the system continuously evacuated by a 160 L/s SIP are presented in **Fig. 7A.9**.

Experimental results clearly show that the outgassing from the insulator on C-1 without AGC is the largest among those under all conditions.

The microdischarge characteristics depending on the elapsed time (**Fig. 7A.7**) are indeed analogous to the outgassing characteristics from the insulator depending on the elapsed time after starting to heat the filament emitter on C-1 (**Fig. 7A.9**). Microdischarges are enhanced by the outgassing from the insulator. The reason is that the insulator surface with a high density of gas molecules causes high-yield secondary-electron emission, leading to positive charging on the insulator surface.

Thermal degassing for the electrodes and insulators has a conditioning effect to reduce microdischarges [7A-9].

Saito et al. (1994) [7A-10] investigated breakdown phenomena in alumina windows for high-power rf use. "Multipactor due to high yields of secondary-electron emission causes F-center oxygen vacancies in the alumina, which induces surface melting. High-purity alumina without micro-porosities or pre-existing F-centers is durable under high-power rf operation. TiN coatings can effectively suppress the multipactor, when the thickness is optimized so as to reduce secondary electrons and to avoid any excessive heating due to rf loss. The surface discharge observed on the TiN-coated surface during higher-power operation indicates the electron-trapping in surface defects and the electron avalanche accompanied by luminescence."

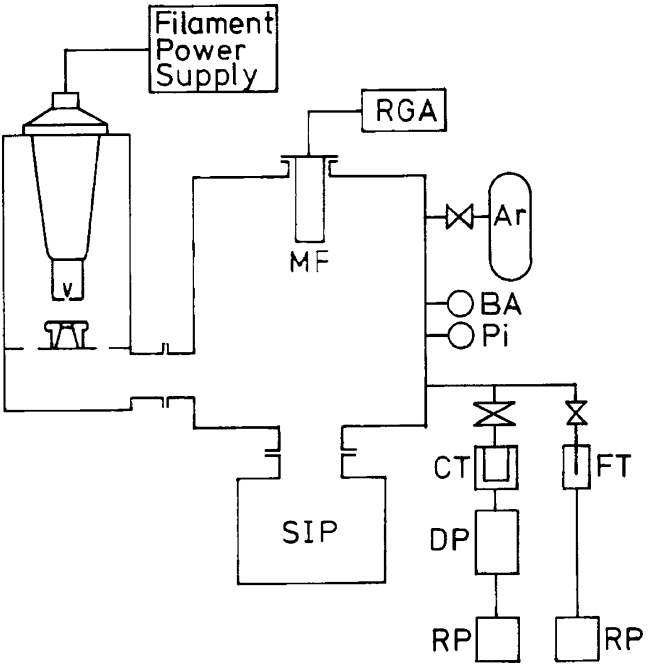

Fig. 7A.8 Ultrahigh-vacuum system with a sputter ion pump. Metal gaskets are used in the high-vacuum side, with the exception of a Viton O-ring for attaching the gun. RGA, residual gas analyzer; MF, quadrupole mass filter; SIP, sputter ion pump (160 L/s); BA, Bayard-Alpert ionization gauge; Pi, Pirani gauge; CT, cold trap; FT, foreline trap; DP, oil diffusion pump, and RP, mechanical rotary pump (Watanabe et al., 1987) [7A-9]

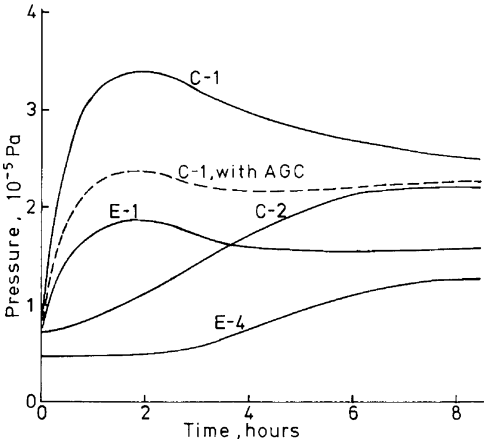

Fig. 7A.9 Pressure-changes in the SIP system after heating the filament emitter with about 10 W. The system was continuously evacuated by the SIP (160 L/s). C-1, 1st day after cleaning without AGC; E-1, 1st day after exposing the chamber to the atmosphere without AGC (Watanabe et al., 1987) [7A-9]

Triple Junction

Shannon et al. (1965) [7A-11] reported that the shape of the cathode triple junction and so the electric field around the junction is very important to obtain the highest insulating performance.

Flashover Strength of Various Insulator Geometries [7A-11]

The high-voltage performances of typical insulator designs are summarized in **Fig. 7A.10**. Both 7070 and 7740 Pyrex glasses were used. In each bar on the chart the thin horizontal line indicates the voltage at which the first spark occurred. Higher up on the bar, a heavier horizontal line indicates the level of insulating (5 min steady value) performance after ten conditioning sparks. The top of the bar indicates the highest insulating voltage obtained.

In this work on the comparative performance of various insulator designs, it is essential that the limitations recorded be due solely to insulator flashover. Therefore, as a preliminary step, it was demonstrated experimentally that an open 25 mm gap between the two stainless-steel electrodes was capable of insulating 250 kV with less than 5×10^{-10} A of inter-electrode current, and that 300 kV could be reliably insulated without sparking. The glass itself has a volume puncture strength in excess of 500 kV/cm. No signs of volume puncture ever were detected in this work.

It was found that the first flashover voltage, as well as the behavior during the initial phase of conditioning, was significant and deserved to be carefully observed, especially

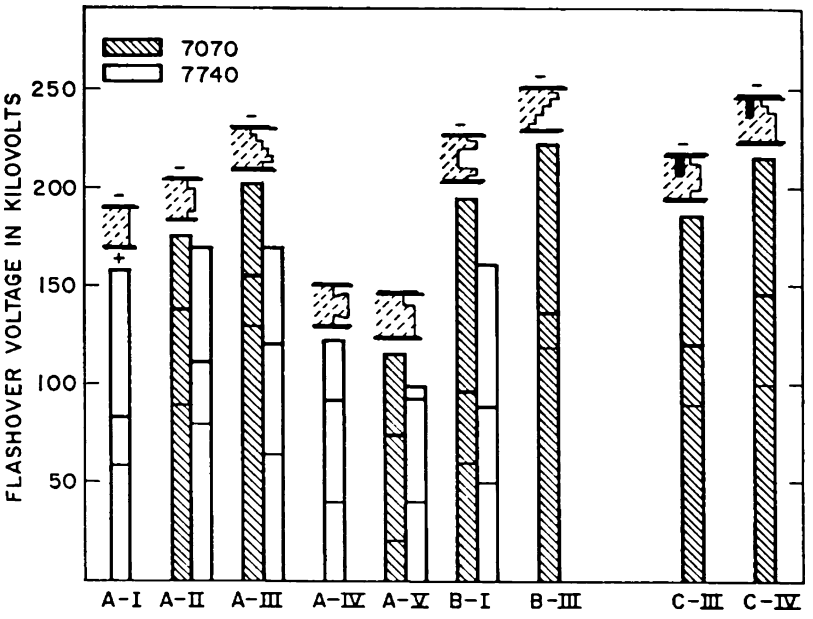

Fig. 7A.10 Flashover strength of various insulator geometries in vacuum. On each bar, the light horizontal line indicates the voltage at which the first flashover took place, the heavy horizontal line the highest voltage which could be held for 5 min after 10 conditioning sparks. The top of each bar indicates the highest voltage which could be held for 5 min after full conditioning (Shannon et al., 1965) [7A-11]

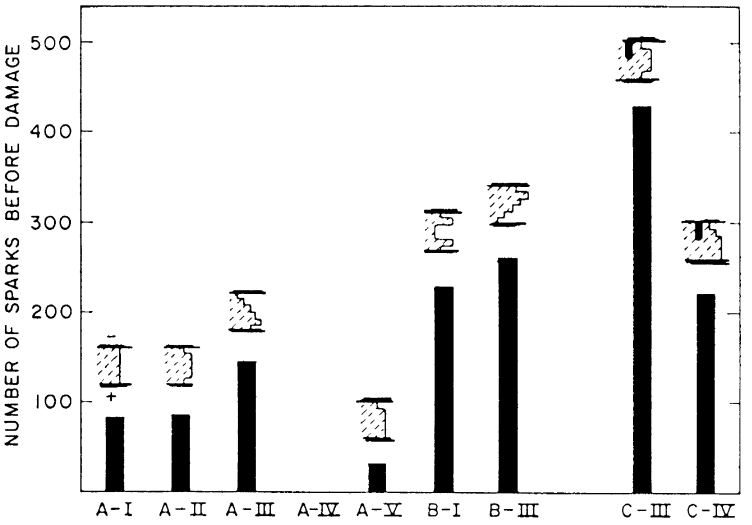

Fig. 7A.11 Number of sparks required to damage various different insulator geometries of 7070 Pyrex glass (Shannon et al., 1965) [7A-11]

since in practice many insulators cannot be conditioned by repeated flashover. The conditioned performance after 30 or more sparks was, in most cases, satisfactorily reproducible.

The ability of an insulator to undergo repeated flashover without damage is of obvious advantage in most applications. Moreover, this resistance to damage is related to its ability to condition to a high insulating strength.

Figure 7A.11 displays the total number of sparks required to damage irreversibly the various different insulator designs. A correlation appears to exist between good insulating performance after conditioning and the ability to experience repeated flashover without damage.

Watson (1967) [7A-12] presented an article, "Pulsed flashover in vacuum."

Abstract [7A-12]: Experiments on the vacuum flashover of dielectric frusta subjected to 35 and 75 ns pulses show the strong influence of cone angle on insulation strength. A theory is presented to explain the formative process leading to flashover for one polarity. It is proposed that positive surface charge grows by emission of hot electrons during the application of the electric field. When the surface field intensity is sufficient to draw other electrons into it, they will multiply by secondary emission until the critical breakdown condition is achieved. Flashover is thus initiated by secondary emission, but the formative time lag is governed by thermionic emission of electrons. The experimental data are analyzed and interpreted in the light of this theory.

Experimental results show the strong influence of cone angle on insulation strength (**Fig. 7A.12**).

Yamamoto et al. (1996) [7A-13] examined the charging of an insulator with double ribs or a recess by using a two dimensional Monte-Carlo simulation method based on the secondary emission electron avalanche (SEEA) mechanism.

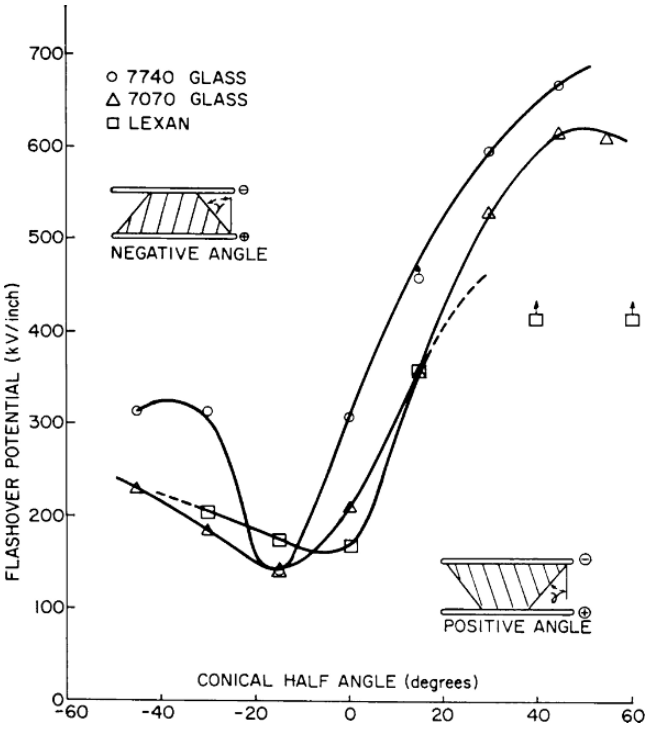

Fig. 7A.12 The flashover strength of glass and Lexan (G.E. polycarbonate resin) as a function of geometry. Tests were first made in the positive-angle configuration and the polarity was reversed to obtain negative-angle data (Watson, 1967) [7A-12]

Abstract [7A-13]: The electric field distribution on a cathode around a triple junction was analyzed taking the charge accumulation into account. Results were compared to those obtained for a simple cylindrical insulator and also insulators with a single rib. Flashover tests were also conducted by using dc voltage. The results of these investigations imply that the number of ribs is unimportant, and that the recess on an insulator is not so effective for the insulation of bridged vacuum gaps.

Surface Flashover in SF_6 Gas

Before the restriction on use of chlorofluorocarbons, high-voltage generator circuits were assembled in a gas tank containing pressurized Freon 12 (CCl_2F_2) gas. After that, they have been assembled in a gas tank containing pressurized SF_6 gas.

Nakanishi et al. (1982) [7A-14] presented an article, "Surface flashovers along insulators under non-uniform electric fields in SF_6 gas". "Many breakdown-voltage

characteristics, such as ac-voltage breakdown characteristics and dc-voltage breakdown characteristics, are presented for the two cases, one with a negative-voltage protrudent electrode and the other with a positive-voltage protrudent electrode."

Review

Hawley (1968) [7A-15] reviewed 26 articles on solid insulators in vacuum.

Abstract [7A-15]: After reviewing the pre-breakdown phenomena (leakage currents, outgassing and luminosity) that arise across a solid insulator held between two electrodes in a vacuum gap, the factors that affect the magnitude of the breakdown voltage (conditioning, electrode and insulator material and surface finish, insulator length and shape, pressure, etc.), the phenomena occurring in the region of the cathode-insulator junction and the hypotheses put forward to explain the breakdown mechanism, are discussed.

Miller (1989) [7A-16] reviewed 99 articles on surface flashover of insulator.

Abstract [7A-16]: Surface flashover of insulators in vacuum generally is initiated by the emission of electrons from the cathode triple junction (the region where the electrode, insulator, and vacuum meet). These electrons then usually multiple as they traverse the insulator surface, either as a surface secondary electron emission avalanche, or as an electron cascade in a thin surface layer, causing desorption of gas which has been adsorbed on the insulator surface. This desorbed gas is then ionized, which lead to surface flashover of the insulator. Some suggestions are made regarding how to choose the material geometry, and processing when selecting an insulator for a particular application.

7B Microdischarges between High-Voltage Electrodes

Anode-Initiation Mechanism

High-voltage breakdown across electrode gaps is explained by the anode-initiation model for high-voltage, low electric-field systems with wide gaps.

Cranberg (1952) [7B-1] presented an article, "The initiation of electrical breakdown in vacuum."

Hypothesis of Cranberg [7B-1]
The hypothesis is that the initiation of breakdown is due to detachment by electrostatic repulsion of a clump of material loosely adhering to one electrode, but in electrical contact with it; traversal by the clump of most or all of the high-voltage gap, and impingement on an electrode at much lower, or at the lowest potential.

A quantitative formulation of this initiation hypothesis may be set down very simply as follows. Assume that breakdown will occur when the energy per unit area W delivered to the target electrode exceeds a value C', a constant, characteristic of a given pair of electrodes. This quantity W is just the product of the gap voltage V by the charge density on the clump. The latter is proportional to the field E at the electrode of origin so that the breakdown criterion becomes simply

$$VE \geq C, \tag{7B.1}$$

where C is a product of C', some numerical factors, and possibly a field-intensifying factor due to microscopic field inhomogeneities in the neighborhood of the clump during detachment from its parent electrode. For the case of plane-parallel electrodes where $E = V/d$,

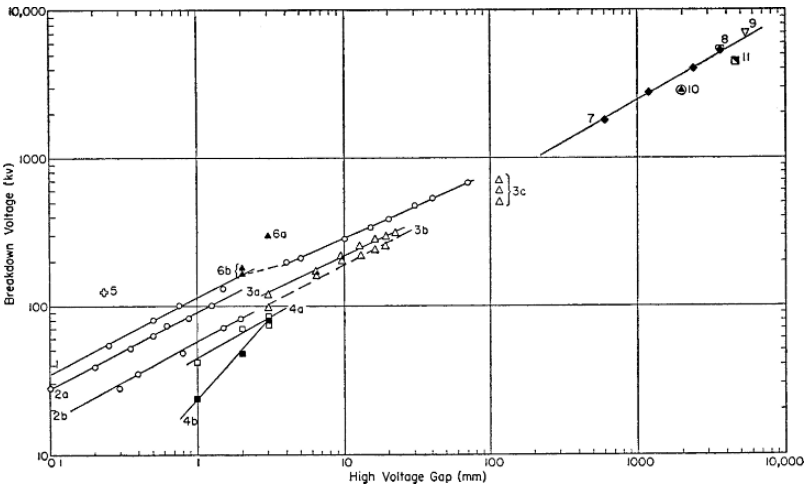

Fig. 7B.1 Plot of data from the literature of breakdown voltage vs. distance from highest to lowest potential electrode, for uniform-field and near-uniform-field geometry. Numbers on curves indicate sources as listed below (Cranberg, 1952) [7B-1]

this criterion predicts at once that the voltage which a gap can sustain is proportional to the square-root of the gap length for a given pair of electrodes.

$$V \propto \sqrt{Cd}. \tag{7B.2}$$

The prediction of this simple result has led to search of the literature for pertinent evidence, a summary of which is given in **Fig. 7B.1** in the form of a log-log plot of voltage vs. length of gap, for uniform and nearly uniform field conditions. The only contradictory evidence is that provided by a three-point curve given by Gleichauf [(P. Gleichauf, *J. Appl. Phys.* **22**, 766, (1951)] for copper electrodes in the range 1–3 mm, whereas all other data are consistent with this prediction.

References

1. J. G. Trump and Van de Graaff, [see J. G. Trump and R. J. Van de Graaff, J. Appl. Phys. **18**, 327 (1947)] 1-inch sphere steel anode, 2-inch steel disk, outgassed with glow discharge.
2. Wm. Parkins, "Vacuum Sparking Potentials under Surge Conditions", *MDDC* **858**, 18 February, 1946. Voltage applied in pulses of 3×10^{-7} sec rise time. (a) Tungsten hemispheres 2-inch diameter, outgassed by spark discharge. (b) Copper hemispheres 2-inch diameter, outgassed by spark discharge.
3. J. L. McKibben and R. K. Beauchamp, "Insulation-Flashover Tests in Vacuum and Pressure", *AECD* 2039. (a) Flat aluminum. (b) Flat cold-rolled steel. (c) Van de Graaff test-section $4\frac{1}{2}$ inches long, aluminum rings sandwiched between Mykroy rings, steel anode plate, negative end open to vacuum system in simulation of operation as beam tube, results on three test-sections.
4. P. Gleichauf [see *J. Appl. Phys*. **22**, 766 (1951)]. (a) Kovar cathode, 18–8 stainless-steel anode, flat with rounded ends. (b) Copper, flat, with rounded ends (hole in center of anode).
5. R. J. Piersol, British Assoc., *Advancement of Science*, Report 359 (1924). Molybdenum spheres after heating to 1400 °C.
6. J. L. Hayden, *Am. Inst. Elec. Engrs. J*. **41**, 852 (1922). (a) Molybdenum spheres 1 cm diameter outgassed to red heat, polished. (b) Molybdenum spheres 1 cm diameter.
7. Los Alamos big Van de Graaff, polished aluminum electrodes.
8. Robinson et al., *Phys. Rev*. (to be published).
9. J. G. Trump (private communication on performance of new 12 MeV Van de Graaff machine, polished aluminum electrodes.
10. Los Alamos small Van de Graaff machine (not limited by tube sparking), steel electrodes.
11. Wisconsin Van de Graaff machine (not limited by tube sparking), steel electrodes.

Chatterton et al. (1972) [7B-2] investigated the role of low-velocity microparticles (diameters$< 100\,\mu$m; velocities $\sim$ 10–50 m/sec) in inducing breakdown in a high-vacuum gap

Abstract [7B-2]: On the basis of a simple model, it is shown that as an anode initiated microparticle approaches the cathode, fields sufficient to cause appreciable field emission ($> 10^9$ V/m) are possible at the cathode surface. The emission current not only causes partial neutralization of the initial charge on the microparticle, but also raises the temperature (>2000 K) of the particle surface. As a consequence, a significant increase in gas pressure ($\sim$ 100 Torr) in the microvolume between the cathode and the particle is possible, resulting in a discharge between the two. Such

a discharge could act as a trigger for the breakdown of the main gap. Other possible processes that could arise due to the onset of melting or boiling of the bombarded surface, and which may lead to breakdown of the entire gap, are also discussed.

Davies (1973) [7B-3] reviewed the recent investigations of prebreakdown conduction phenomena in vacuum both for steady and for step-function applied voltages.

Abstract [7B-3]: The results of these investigations have led to the formulation of models to explain the initiation of the vacuum discharge by ionization of a vapor medium, the vapor being composed of atoms of one or both of the electrodes. A detailed examination of the events leading to breakdown has allowed a more critical evaluation of the merits and deficiencies of the various breakdown models.

Menon and Srivastava (1974) [7B-4] presented an article, "Microparticle-initiated vacuum breakdown-Some possible mechanisms."

Abstract [7B-4]: It is known that micron- and submicron-sized metallic particles are released from the electrode surfaces when a vacuum gap is subjected to a high dc stress. It is also well known that larger particles ($> 10\,\mu m$) are generated within the inter-electrode gap when a vacuum gap is subjected to conditioning or severe prebreakdown current flow. This paper examines the role of such particles in inducing the breakdown of a vacuum gap. While the larger particles induce breakdown by way of a trigger discharge, it is shown that the smaller particles ($< 3\,\mu m$) can initiate breakdown because of effects associated with impact. The various effects associated with the high-speed impact of a metallic microparticle on a target electrode, viz., cratering, production of metal vapor, and production of thermally generated plasma and their relative significance on vacuum breakdown, are examined.

Davies and Biondi (1977) [7B-5] presented an article, "Emission of electrode vapor resonance radiation at the onset of dc breakdown in vacuum."

Abstract [7B-5]: Simultaneous time-resolved spectroscopic and current measurements have been made during the early stages of current growth leading to dc breakdown in vacuum between plane-parallel electrodes of dissimilar material. These measurements show that resonance-radiation characteristic of anode material is emitted prior to that of cathode material from all regions of the inter-electrode gap. Further, the radiation is emitted first from the cathode region of the gap. The results indicate that the initial current growth occurs in anode vapor followed at later times by the appearance of cathode vapor in the gap.

Allen et al. (1979) [7B-6] presented an article, "The source of high-β electron emission sites on broad-area high-voltage alloy electrodes."

Abstract [7B-6]: Two recently developed techniques have been used sequentially in an attempt to define the nature of high-β (β, field-increase factor) field-emission sites on a commercial-alloy, broad-area, electrode surface. The techniques involved were: (1) an in situ electron-optical method for locating and examining the emission site; and (2) a high-resolution spectrometer for determining the energy spectra of the electrons field emitted from this site. Furthermore, following these measurements, the elemental composition of the emission area was determined by electron microprobe x-ray analysis. Observations, which cast further doubt upon the

traditional concept of field-enhancing micro-projections, indicate that the sites are non-metallic and probably consist of impurities located at cracks or grain boundaries in the surface. Tentative hypotheses are proposed for the emission mechanism and include provision for an unstable situation caused by the effects of adsorbed gas atoms.

Diamond (1998) [7B-7] presented an article, "New perspectives in vacuum high voltage insulation. I . The transition to field emission."

Abstract [7B-7]: Field emission is not present at all fields, but typically starts after some process occurs at the cathode surface. Three effects have been identified that produce the transition to field emission: work function changes; mechanical changes produced by the strong electrical forces on the electrode surfaces; and gas desorption from the anode with sufficient density to support an avalanche discharge. Localized regions of low work function can be produced on the cathode by the transfer of microparticles from the anode and by stripping small areas of the cathode. The regions of low work function then serve as the source of enhanced field emission, leading to secondary effects which produce breakdown. Gas desorption is produced at an unconditioned anode as the voltage is increased. None of these effects are significant for a point cathode opposite a broad-area anode, but account for much of the large difference between microscopic and macroscopic breakdown fields [7B-7].

Diamond (1998) [7B-8] also presented an article titled "New perspectives in vacuum high voltage insulation. II. Gas desorption."

Abstract [7B-8]: An examination has been made of gas desorption from unbaked electrodes of copper, niobium, aluminum, and titanium subjected to high voltage in vacuum. A very significant observation was that the gas desorption was more dependent on the total voltage between the electrodes than on the electric field. It was not triggered by field-emitted electrons but often led to field emission, especially at large gaps. The physical processes that lead to voltage-induced desorption are complex, but there is strong evidence that the microdischarges are the result of an avalanche discharge in a small volume of high-density vapor desorbed from the anode. The source of the vapor may be water or alcohol stored as a fluid in the many small imperfections of the polished metal surface. Microdischarges can then trigger field-emitted electrons which, in turn, heat a small area of the anode. As the temperature of this region of the anode reaches about 500 °C, some fraction of the desorption products are ionized positively and accelerated to the cathode, producing secondary electrons with a yield greater than unity per incident ion. The positive ions appear to originate from the bulk of the metal rather than from surface ionization and the yield increases exponentially with temperature, rapidly producing a runaway condition, i.e., electrical breakdown. These observations support a new perspective on vacuum-high-voltage insulation and produce new insight into vacuum outgassing of metals.

Ion-Exchange Process and Total-Voltage Effect

Cranberg and Henshall (1959) [7B-9] investigated to determine the conditions under which the voltage sustained by a 2 ft length of ion-accelerator tube may be made proportional to the length of the tube.

Abstract [7B-9]: It has been found that such linearity may be obtained if the tube is segmented at $4\frac{1}{2}$ in. intervals by diaphragms which are so arranged that no straight path is possible from one end of the tube to the other. No significant deterioration in performance of the tube was observed when axial holes were made in each diaphragm up to $3/4$ in. in diameter. The voltage gradient realized on these tests was 60 kV/cm.

Mansfield (1960) [7B-10] presented an article, "Pre-breakdown condition in continuously-pumped vacuum systems."

Abstract [7B-10]: Measurement have been made under impulse conditions of the coefficients A', the number of H^+ ions emitted per 250 keV H^- ion, and B', the number of H^- ions emitted per 250 keV H^+ ion, for metal surfaces covered with the contaminating layers likely to be formed in continuously pumped high-voltage apparatus. The values obtained for A' were 1.0, 1.1 and 0.54, and for B' 0.43, 0.24 and 0.44 for copper, aluminum and steel targets, respectively. The product of these coefficients is such as to make very probable the hypothesis that pulse discharge conduction in these system is due to the regenerative exchange of positive and negative ions of hydrogen. The transient nature of this form of conduction is thought to be due to the charging up of the insulating contaminant.

Powell and Chatterton (1970) [7B-11] examined the prebreakdown conduction between stainless steel, copper, aluminum and tungsten electrodes at small gaps (less than 1 cm) and in poor (10^{-6} Torr, unbaked) and clean (3×10^{-9} Torr, baked) vacuum systems.

Abstract [7B-11]: Emphasis has been placed on means of distinguishing between the various types of conduction found to occur. These were identified as (1) field emission and an associated current pulse structure, (2) field emission and activation/ignition effects, (3) microdischarges. This identification was possible directly as a result of using a fast response current measuring system. Equally, the determination of true field emission characteristics, especially in the poor vacuum system, in the presence of the pulse structure and activation/ignition effects was achieved only by means of an ageing process and a fast I-V plotter. The role of surface contamination in determining apparent emission law characteristics has been recognized and a simple, qualitative model proposed which can account for many of the observed effects.

Prichard (1973) [7B-12] studied high-voltage (up to 400 000 V) electrical discharge mechanisms in a stainless-steel and alumina-ceramic vacuum system evacuated by an orbitron getter-ion pump.

Abstract [7B-12]: Mass-spectrometer studies were made of ions emitted from the terminal during discharges with positive and negative terminal polarities. Ions

ejected from the terminal by a beam of Na^+ ions were also examined. Results of these and other studies led to the conclusion that the regularly spaced discharge pulses were the result of an ion-exchange multiplication process. Measurements demonstrate that the gas hinders this mechanism by stripping electrons from negative ions. Electrons were found to be only by-products in the multiplication process. In contrast to the whisker mechanism, the ion-exchange multiplication was found to depend only on total voltage and not on electric-field strength. Experiments with gaps smaller than 2 in. supported the conclusions that the voltage is limited by field emitting whiskers and the presence of gas which damages these whiskers.

Takaoka et al. (1982) [7B-13] presented an article, "Electron energy analysis of vacuum discharge in high-voltage accelerator tube."

Abstract [7B-13]: Measurement of electron energy spectra is useful for diagnosis of vacuum discharge in accelerator tubes. This gives the starting positions of discharge electrons. One block of the accelerator tube of 3 MV electron microscope was tested. Experiments confirm that the main process of discharge is ion-exchange between the top and bottom plates. For three models of electrode shapes, the possibility of secondary-electron multiplication in the 3 MV tube was discussed from the standpoints of both the measured energy spectra and the calculated secondary-electron trajectories. The results were consistent with the actual features of discharge in the 3 MV tube.

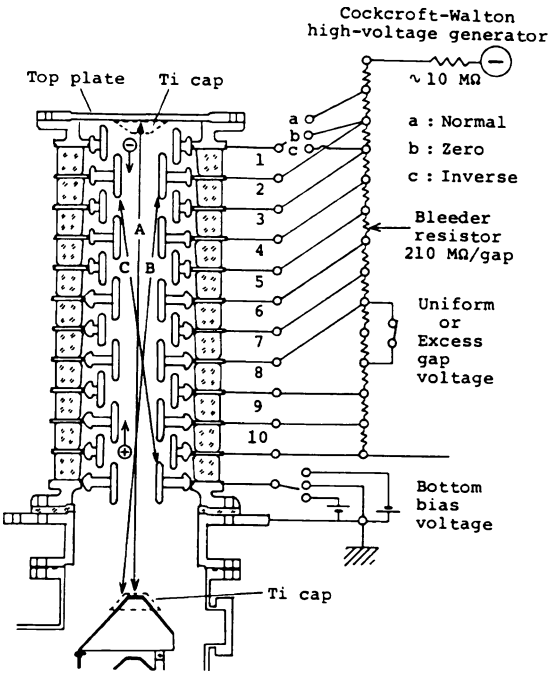

Fig. 7B.2 Application of gap and bias voltages and paths of ion-exchange (Takaoka et al., 1982) [7B-13]

Energy Spectra in the Case of Secondary-Ion Suppression [7B-13]
If the discharge process is ion-exchange, it may be effective, as mentioned by Eastham et al., [1] to suppress the secondary-ion emission due to ion bombardment at the top and bottom plates. Retarding potentials for secondary ions were applied as shown in the right-hand circuit of **Fig. 7B.2**. The potential of the top electrode can be switched to three different values which correspond to the different positions of the bleeder resistors. The bottom bias voltage is applied to the lowest electrode as shown in **Fig. 7B.2**. The switch in the 8th gap is usually closed.

Figure 7B.3 shows the relation between the threshold voltage and the bias voltages. In this figure, the legend "normal", "zero" or "inverse" corresponds to the switch position for the top plate as shown in **Fig. 7B.2**. The threshold voltage does not change for positive bias on the bottom electrode which corresponds to a retarding field for positive secondary ions, while it decreases greatly as the negative bias increases. The field inverse (field retarding secondary ions) to the top plate hardly improves the threshold voltage at all but relaxes the effect of the negative bottom bias as seen in **Fig. 7B.3**.

Figure 7B.4 shows the energy spectra corresponding to three different bias voltages applied to the top plate for the case of a uniform gap voltage. As seen from **Fig. 7B.2**, the odd-numbered electrodes are remote from the tube axis, compared to the even-numbered

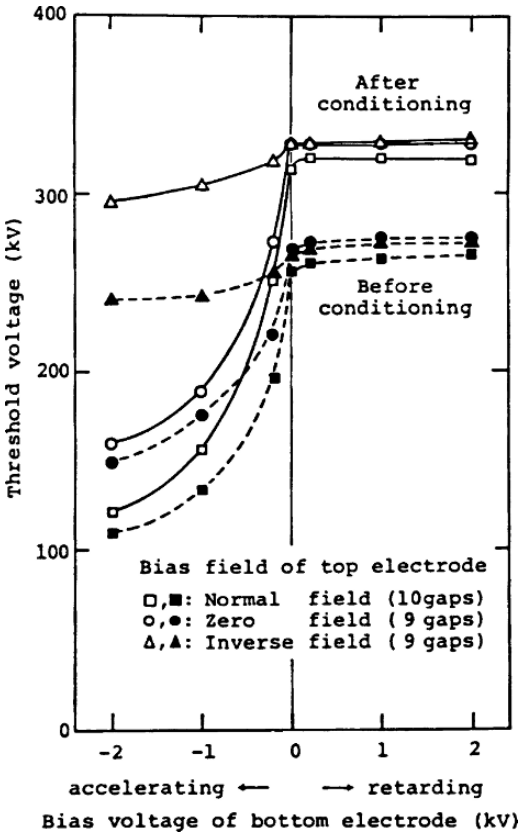

Fig. 7B.3 Threshold voltage as a function of the bias voltage at the top and bottom electrodes (Takaoka et al., 1982) [7B-13]

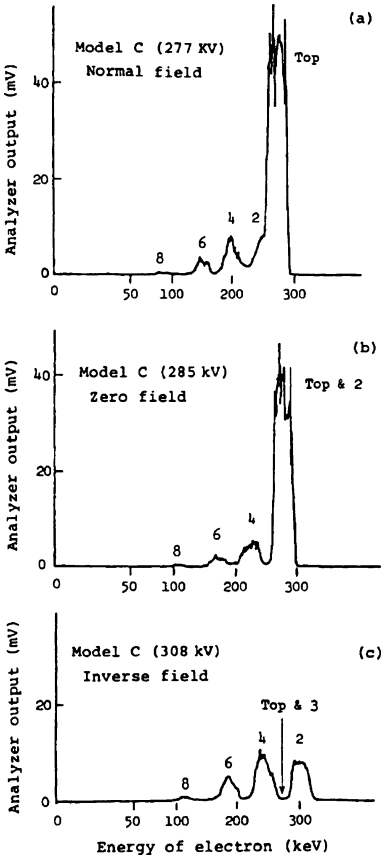

Fig. 7B.4 Electron-energy spectra in the case of uniform gap voltage; the top bias voltage is **(a)** normal field, **(b)** zero field and **(c)** inverse field (Takaoka et al., 1982) [7B-13]

electrodes. Hence, odd-numbered peaks except for the first are not observed in the energy spectra as seen in **Fig. 7B.4**; the first peak corresponds to the electrons from the top plate.

In the cases of the normal and zero fields, most of the electrons come from the top electrode. This implies that the path predominantly used for ion-exchange would be path "A" in **Fig. 7B.2**, that is, the longest path. On the other hand, in the case of the inverse field, the potential of the top plate is the same as that of the 3rd electrode. Therefore, if an electron comes from the top plate, it should be found on the same energy level as the 3rd electrode in the energy spectrum. It is seen in **Fig. 7B.4 (c)** that the energy of the electron from the top plate is drastically reduced. This implies that the secondary negative ion from the top plate would be similarly suppressed by the retarding field. That is, in this case, the most predominantly used path "A" of ion-exchange may disappear due to the retarding field.

Figure 7B.5 shows the energy spectra when a three-fold excess voltage is applied to the 8th gap by the opening of the switch in **Fig. 7B.2**. The excess voltage would act as a trigger for discharge. Here, the bias voltages are applied to both ends, whereas in the case of **Fig. 7B.4**, only the top plate is biased. **Figure 7B.5 (a)** shows the energy spectrum when the bias voltage for both ends is zero. The peak corresponding to the discharge at the 8th gap is clearly observed, although the highest peak is at the highest energy. **Figure 7B.5 (b)**

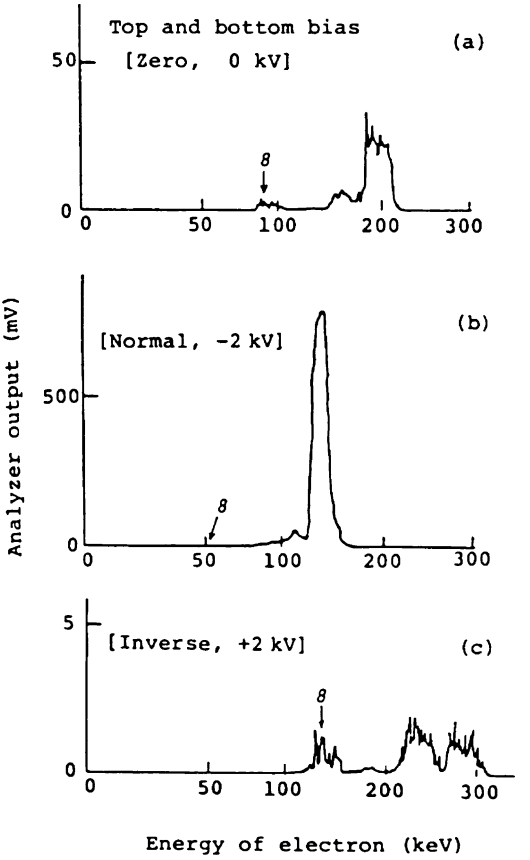

Fig. 7B.5 Electron-energy spectra in the case of excess voltage at the 8th gap; the top and bottom bias voltage are **(a)** zero, **(b)** normal and –2kV and **(c)** inverse and +2kV, respectively (Takaoka et al., 1982) [7B-13]

shows the energy spectrum in the case of the normal top bias and negative bottom bias; in this case the secondary-ion emission is enhanced. The peak corresponding to the 8th gap is scarcely observed, because the threshold voltage decreases to the same extent as the trigger discharge in the 8th gap disappears. It is notable that the peak values at the highest energy are one order higher than that of **Fig. 7B.5 (a)** and that the energy spectrum is more confined to the highest energy than the case in **Fig. 7B.4 (a)**. These features were commonly observed when the applied voltage was lower than the conditioning voltage. When the retarding fields for secondary ions are applied to both end plates, the peak value at the highest energy is depressed, as shown in **Fig. 7B.5 (c)**, by about one order as compared with **Fig. 7B.5 (a)**.

The above results are consistent with the supposition that the main discharge process occurring in the accelerator tube would be ion-exchange. If this is assumed, the reason why the threshold voltage did not increase in line with the retarding field as seen in **Fig. 7B.3** can be explained also as follows. At first, in **Fig. 7B.2** we (Takaoka et al.) consider some paths for ion-exchange, for example, paths “A”, “B” and “C”. We may assume that the ion-exchange multiplication factors of these paths are unity during the conditioning process. Indeed, if this factor for a certain path is more than unity, the electrode surfaces corre-

sponding to this path would be selectively aged by the ion-exchange process until unity is achieved. On the contrary, if the factor is less than unity, the corresponding surfaces would not be aged and this factor would achieve unity as the conditioning voltage increased. Even if the ion-exchange for the longest path "A" disappeared due to the retarding field, another path "C", for example, would remain because the retarding field does not affect path "C". In this case, the threshold voltage is unaltered. Furthermore, it seems that the drastic reduction at the highest energy level in **Fig. 7B.5 (c)** corresponds to the reduction of surface area contributing to ion-exchange; the surface area contributing to path "C" is much smaller than that to path "A".

Reference

1. D. A. Eastham and R. Thorn, *J. Phys. D*: *Appl. Phys*., **11**, 1149 (1978)

Projection (Whisker) on Cathode

Peter (1984) [7B-14] presented an article, "Vacuum breakdown and surface coating of rf cavities."

Abstract [7B-14]: Electrode surface coating may play an important part in overcoming power limitations in rf cavities for voltages far above the electron multipacting limit. In such cases, the principal use of the coating is not to reduce secondary emission but to isolate electrode whiskers from the cavity chamber and to serve as a trap for slow electrons. Restrictions on the layer thickness are derived theoretically, and calculated for conventional accelerator cavities.

Miller (1984) [7B-15] presented an article, "Influence of gap length on the field increase factor β of an electrode projection (whisker)."

Abstract [7B-15]: β, the increase factor of the macroscopic electric field at the tip of a projection, varies with the gap length. The sign and magnitude of this variation depends upon how the gap length is defined. If gap length is defined as x, the distance from the projection tip to the opposing electrode, then β is a strong function of x and may be approximated by $\beta(x) = \beta_\infty x/(x+h)$ [h = projection height] in the region where $x/h > 10/\beta_\infty$. If gap length is defined as d, the inter-electrode distance ignoring the projection, then β is a weak function of d and may be set equal to β_∞ in the region $d/h > 2$.

Gas Molecules on Electrode Surfaces

The breakdown voltage becomes higher after a voltage higher than the rated voltage has been applied for a while to a high-voltage electrode (this is called "high-voltage conditioning"). A similar effect is achieved after the surfaces of high-voltage electrodes have been bombarded with energetic ions and electrons. Baking of electrode

and insulator surfaces also has a conditioning effect. So-called "conditioning" is considered a kind of degassing.

Yoshimura et al. (1987) [7B-16] examined the conditioning effect of Ar-glow conditioning (AGC; 350 Vac, 180 mA, 5 min in about 10 Pa of Ar) for microdischarges between high-voltage electrodes.

Ar-Glow Conditioning

Effect of Ar-Glow Conditioning [7B-16]

The Wehnelt electrode and insulator of the electron gun (**Fig. 7A.6**) were first cleaned using CH_3CCl_3 solvent, and microdischarges were examined under high vacuum before and after AGC. Experimental results, together with the experimental process, are presented in **Fig. 7B.6**.

When –100 kV was first applied to the Wehnelt electrode under a high vacuum in the 10^{-4} Pa range, microdischarges of about 10 V (peak to peak) occurred immediately. On the other hand, no microdischarge occurred after the gun had been treated with AGC. However,

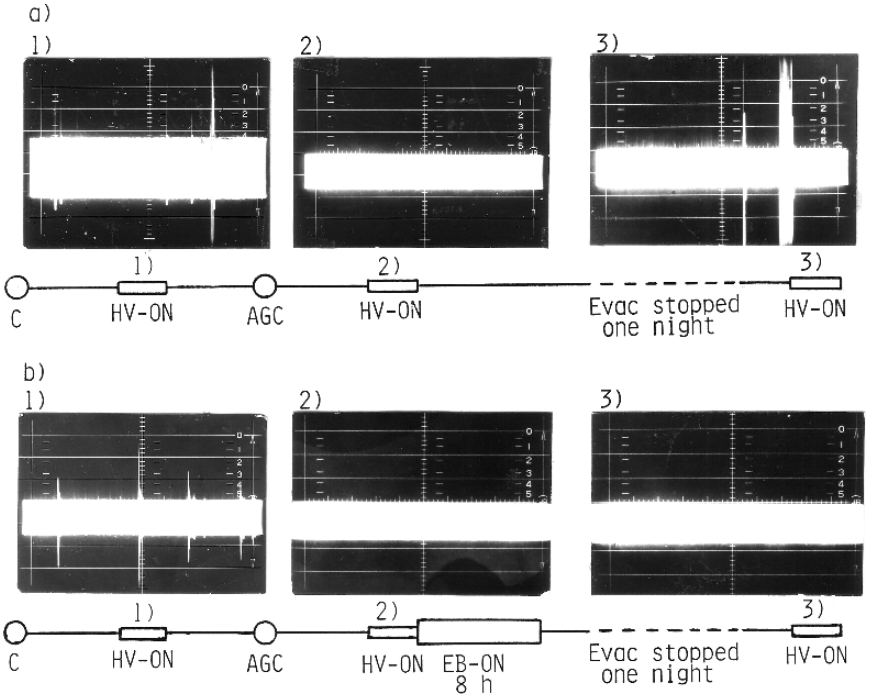

Fig. 7B.6 Microdischarges in the 10^{-4} Pa range before and after AGC. **(a)** Electron beam (EB) off, and **(b)** EB on (about 50 μA, about 8 h). Sensitivity and scanning speed of CRT are 1 V/div. and 10 s/frame, respectively (Yoshimura et al., 1987) [7B-16]

even after AGC, microdischarges again occurred under a high vacuum on the next day after the gun had been held in the vacuum chamber isolated from the vacuum pump for one night (see **Fig. 7B.6 a**). Next, in another process, an electron beam (EB) of about 50 μA was extracted from the filament emitter for about 8 h under about 10^{-4} Pa following AGC. In this case, microdischarges did not occur on the next day (see **Fig. 7B.6 b**). The Wehnelt electrode and the insulator (a kind of porcelain whose surface is treated to be glassy) had to be thermally degassed by the heat (about 10 W) from the filament emitter. Thermal degassing for the electrodes and insulators has a conditioning effect to reduce microdischarges between the electrode and over the insulator surface.

High-Voltage Conditioning (HVC)

Effect of High-Voltage Conditioning [7B-16]

High-voltage conditioning (HVC) in high vacuum is a well-known treatment for high-voltage electrodes. Several kV ac superimposed on about 110 kV dc is generally used in HVC for an electron gun of 100 kV. However, high-voltage ion bombardment sometimes damages the electrode and the insulator. Also, the durability of the effect of HVC is rather short.

Example data on the durability of the effect of HVC, applied to an electron gun of an old electron microscope, are presented in **Fig. 7B.7**. The gun is similar in construction to the one shown in **Fig. 7A.4**. These data were obtained after evacuating the electron microscope for a short time.

As seen in **Fig. 7B.7**, the durability is considerably short, so repeated HVC is generally necessary. The short durability is caused by the fact that only a limited small area of the electrodes is bombarded with ions and electrons. Also, as is seen in **Fig. 7B.8)**,

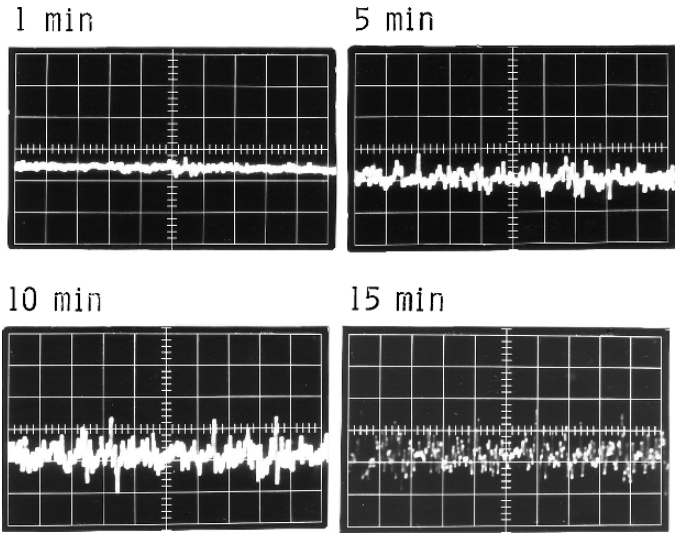

Fig. 7B.7 Durability of the effect of HVC applied to an electron-microscope gun. Sensitivity and scanning speed of CRT are 1 V/div. and 10 s/frame, respectively (Yoshimura et al., 1987) [4B-16]

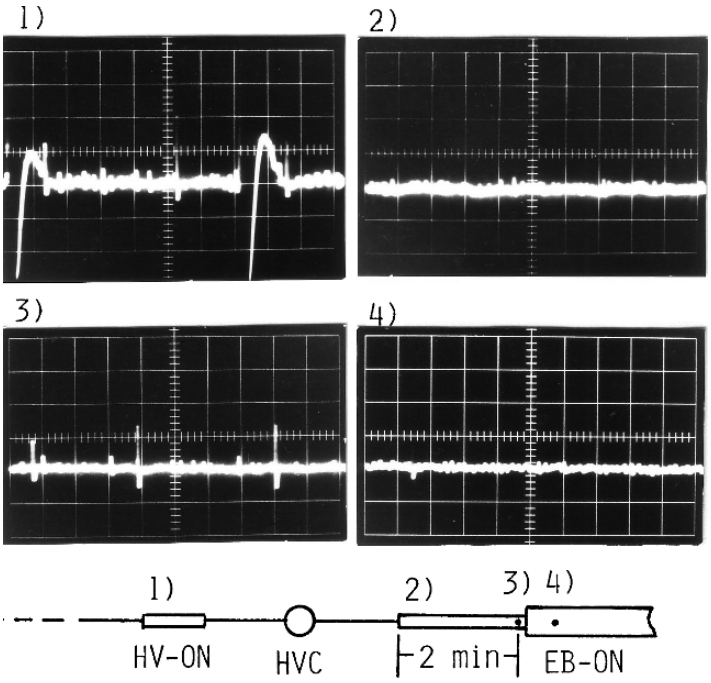

Fig. 7B.8 Microdischarges between the electrodes in 10^{-4} Pa range before and after HVC. Sensitivity and scanning speed of CRT are 1 V/div. and 10 s/frame, respectively (Yoshimura et al., 1987) [7B-16]

microdischarges diminish during electron beam extraction. It is considered that when an electron beam is being extracted, the electric field at the vicinity of the hole of Wehnelt electrode becomes low, diminishing microdischarges.

Kobayashi et al. (1996) [7B-17] investigated the effects of heating electrodes, and diamond turning of electrode surfaces (oxygen-free copper) to a mirror finish upon electrical breakdown in a vacuum.

Abstract [7B-17]: It was found that the mirror finish obtained by diamond turning reduces the number of repetitive breakdowns to achieve higher hold-off voltages. Heating treatment for the electrodes was effective in improving the breakdown strength after the conditioning process. A higher heating temperature produced a higher breakdown field. A breakdown field of about 250 MV/m was obtained for electrodes heated at 700 °C in a vacuum and then finished by diamond turning. It has been concluded that an improvement in the breakdown field by heating is due to the reduction of the gas contents rather than recrystallization.

Conditioning Effect

There are the interesting views on the effect of conditioning, which were presented by Hawley (1968) [7A-15] and Peter (1984) [7B-14], respectively.

Hawley's View on Conditioning [7A-15]

As in a plain vacuum gap, the phenomenon of conditioning takes place whereby the electrical strength improves during successive breakdowns. Gleichauf [1] investigated the general behavior of the conditioning process, the part played by the electrodes and the part played by the insulators on the conditioning process and he (Gleichauf) also studied the effect on conditioning of the circumstances under which the breakdown arc extinguished. He (Gleichauf) found that with successive breakdowns the breakdown voltage followed a general trend towards higher voltages, the rate of increase diminishing with time. When the voltage was removed for a while, part of the conditioning was lost but the insulator subsequently reconditioned at a faster rate. The degree of conditioning lost was dependent on the previous history of the insulator. As the time interval between the successive series of tests was increased, the initial breakdown voltage on resumption of testing decreased but was usually of a higher value than the very first breakdown voltage for the insulator. The same loss of conditioning was found if the insulator was taken from the continuously pumped vacuum chamber and exposed to the atmosphere, the length of exposure to the atmosphere being immaterial.

Reference

1. P. H. Gleichauf, *J. Appl. Phys.* **22**, 535, 1951.

Peter's View on Conditioning [7B-14]

An important factor in breakdown-voltage levels appears to be the extent of conditioning of the electrode surfaces [1, 2, 3]. Conditioning is achieved by low-current glow discharges, repeated sparking, or gradual increases in the applied voltage. An interesting theory proposed by Halbritter [4] suggests that the reduced electron emission from conditioning is due to the polymerization of adsorbed hydrocarbons on the electrode surfaces. Such layers show strong inelastic scattering for slow electrons, effectively reducing the secondary emission and field emission out of excited states. Another theory is that conditioning is responsible for blunting the micron-length whiskers that grow on metal surfaces when high voltages are applied [3].

There is some evidence [4] that the polymerized hydrocarbon layers show strong inelastic scattering for slow electrons, thereby reducing emission out of this layer for both field-emitted and secondary electrons. According to this theory, voltage thresholds may be raised even higher by rinsing surfaces with hydrocarbon-based materials in a dust-free environment [4]. This decrease in emission by the application of a thin ($<$10 Å) absorbing medium for slow electrons is different from the use of a thick surface coating (about 1000 Å) to isolate electrode whiskers from vacuum or to decrease secondary emission. In the former case, for example, the actual yield of secondary emission is decreased; in the latter case, increased inelastic scattering suppresses secondary emission out of the material. It is possible, therefore, to apply the hydrocarbon layer over the initial (carbon-coated or dielectric) layer to further reduce the possibility of high-voltage discharge.

References

1. Yu. Nikolaev, *Zh. Tech. Fiz.* **33**, 479 (1963). [*Sov. Phys. Tech. Phys.* **8**, 354 (1963).]
2. D. Boehne, W. Karger, E. Miersch, W. Roske, and B. Stadler, *IEEE Trans. on Nucl. Sci.* **18**, 568 (1971).

3. D. W. Reid and R. A. Lohsen, *Los Alamos Scientific Laboratory report* LA-UR-82-2400, October, 1982.
4. J. Halbritter, *J. Appl. Phys*. **53**, 6475 (1982).

Comment: Peter's view, that the conditioning accompanied by discharge creates the surfaces of electrode with low emission efficiency of secondary electrons, is very interesting. As described in "5C Darkening in Secondary Electron Images" secondary-electron emission from the area pre-irradiated with a fine electron probe is much reduced. Also, surfaces covered with polymerized thin films show lower secondary-electron emission compared with the original surfaces.

Review

Oostrom and Augustus (1982) [7B-18] reviewed 46 articles on electrical breakdown between stainless-steel electrodes in vacuum.

Abstract [7B-18]: Electrical breakdown in vacuum is reviewed, particularly for the case of a small gap (<2 mm) between a pair of stainless-steel electrodes. Theoretical descriptions and experimental results are compared, and it is concluded that field-emitting sites on the cathode are responsible for the electron bombardment of the anode, the subsequent evaporation of anode material and the initiation of a breakdown.

References

Microdischarges over Insulator Surfaces

7A-1. P. H. Gleichauf, "Electrical breakdown over insulators in high vacuum", *J. Appl. Phys.* **22** (6), pp. 766–771 (1951).
7A-2. A. S. Pillai and R. Hackam, "Surface flashover of solid insulators in atmospheric air and in vacuum", *J. Appl. Phys.* **58** (1), pp. 146–153 (1985).
7A-3. C. H. De Tourreil and K. D. Srivastava, "Mechanism of surface charging of high-voltage insulators in vacuum", *IEEE Transactions on Electrical Insulation* **EI-8** (1), pp. 17–21 (1973).
7A-4. T. S. Sudarshan and J. D. Cross, "DC electric-field modifications produced by solid insulators bridging a uniform-field vacuum gap", *IEEE Transactions on Electrical Insulation* **EI-8** (4), pp. 122–128 (1973).
7A-5. R. A. Anderson and J. P. Brainard, "Mechanism of pulsed surface flashover involving electron-stimulated desorption", *J. Appl. Phys.* **51** (3), pp. 1414–1421 (1980).
7A-6. A. S. Pillai and R. Hackam, "Surface flashover of solid dielectric in vacuum", *J. Appl. Phys.* **53** (4), pp. 2983–2987 (1982).
7A-7. J. D. Cross and T. S. Sudarshan, "The effect of cuprous oxide coatings on surface flashover of dielectric spacers in vacuum", *IEEE Transactions on Electrical Insulation.* **EI-9** (4), pp. 146–150 (1974).

7A-8. T. S. Sudarshan and J. D. Cross, "The effect of chromium oxide coatings on surface flashover of alumina spacers in vacuum", *IEEE Transactions on Electrical Insulation* **EI-11** (1), pp. 32–35 (1976).
7A-9. H. Watanabe, N. Yoshimura, S. Katoh, and N. Kobayashi, "Microdischarges on an electron gun under high vacuum", *J. Vac. Sci. Technol. A* **5** (1), pp. 92–97 (1987).
7A-10. Y. Saito, S. Anami, S. Michizono, N. Matuda, A. Kinbara, S. Kobayashi, "Breakdown of alumina rf windows and its inhibition", *T. IEE Japan*, Vol. 114-A, No. 2, pp. 100–107 (1994) (in Japanese).
7A-11. J. P. Shannon, S. F. Philp, and J. G. Trump, "Insulation of high voltage across solid insulators in vacuum", *J. Vac. Sci. Technol.* **2** (5), pp. 234–239 (1965).
7A-12. A. Watson, "Pulsed flashover in vacuum", *J. Appl. Phys.* **38** (5), pp. 2019–2023 (1967).
7A-13. O. Yamamoto, T. Hara, H. Matsuura, Y. Tanabe, and T. Konishi, "Effects of corrugated insulator on electrical insulation in vacuum", *Vacuum* **47** (6–8), pp. 713–717 (1996).
7A-14. K. Nakanishi, Y. Shibuya, Y. Arahata, and T. Eura, "Surface flashovers along insulators under non-uniform electric fields in SF_6 gas", *Transactions of The Institute of Electrical Engineers of Japan A*: *Publication of Fundamentals and Materials Society* **102** (9), pp. 1–8 (1982) (in Japanese).
7A-15. R. Hawley, "Solid insulators in vacuum: A review", *Vacuum* **18** (7), pp. 383–390 (1968).

Microdischarges Between High-Voltage Electrodes

7A-16. H. C. Miller, "Surface flashover of insulators", *IEEE Transactions on Electrical Insulation* **24** (5), pp. 765–786 (1989).
7B-1. L. Cranberg, "The initiation of electrical breakdown in vacuum", *J. Appl. Phys.* **23** (5), pp. 518–522 (1952).
7B-2. P. A. Chatterton, M. M. Menon, and K. D. Srivastava, "Processes involved in the triggering of vacuum breakdown by low-velocity microparticles", *J. Appl. Phys.* **43** (11), pp. 4536–4542 (1972).
7B-3. D. K. Davies, "The initiation of electrical breakdown in vacuum–A review", *J. Vac. Sci. Technol*. **10** (1), pp. 115–121 (1973).
7B-4. M. M. Menon and K. D. Srivastava, "Microparticle-initiated vacuum breakdown–some possible mechanisms", *J. Appl. Phys.* **45** (9), pp. 3832–3835 (1974).
7B-5. D. K. Davies and M. A. Biondi, "Emission of electrode vapor resonance radiation at the onset of dc breakdown in vacuum", *J. Appl. Phys.* **48** (10), pp. 4229–4233 (1977).
7B-6. N. K. Allen, B. M. Cox, and R. V. Latham, "The source of high-β electron emission sites on broad-area high-voltage alloy electrodes", *J. Phys. D*: *Appl. Phys.* **12** (6), pp. 969–978 (1979).
7B-7. W. T. Diamond, "New perspectives in vacuum high voltage insulation. I. The transition to field emission", *J. Vac. Sci. Technol. A* **16** (2), pp. 707–719 (1998).
7B-8. W. T. Diamond, "New perspectives in vacuum high voltage insulation. II. Gas desorption", *J. Vac. Sci. Technol. A* **16** (2), pp. 720–735 (1998).
7B-9. L. Cranberg and J. B. Henshall, "Small-aperture diaphragms in ion-accelerator tubes", *J. Appl. Phys.* **30** (5), pp. 708–710 (1959).
7B-10. W. K. Mansfield, "Pre-breakdown conduction in continuously-pumped vacuum systems", *Brit. J. Appl. Phys.* **11** Oct., pp. 454–461 (1960).
7B-11. H. P. S. Powell and P. A. Chatterton, "Prebreakdown conduction between vacuum insulated electrodes", *Vacuum* **20** (10), pp. 419–429 (1970).
7B-12. B. A. Prichard Jr., "Mechanisms of electrical discharges in high vacuum at voltages up to 400 000 V", *J. Appl. Phys.* **44** (10), pp. 4548–4554 (1973).
7B-13. A. Takaoka, K. Ura, and K. Yoshida, "Electron energy analysis of vacuum discharge in high-voltage accelerator tube", *J. Electron Microsc.* **31** (3), pp. 217–225 (1982).

7B-14. W. Peter, "Vacuum breakdown and surface coating of rf cavities", *J. Appl. Phys.* **56** (5), pp.1546–1547 (1984).
7B-15. H. C. Miller, "Influence of gap length on the field increase factor β of an electrode projection (whisker)", *J. Appl. Phys.* **55** (1), pp. 158–161 (1984).
7B-16. N. Yoshimura, H. Watanabe, S. Katoh, and N. Kobayashi, "Microdischarges on a high-voltage electron gun under high vacuum", *Shinku (J. Vac. Soc. Japan)* **30** (3), pp. 105–115 (1987) (in Japanese).
7B-17. S. Kobayashi, Y. Hashimoto, M. Maeyama, Y. Saito, and Y. Nagai, "Electrical breakdown strength of oxygen-free copper electrodes under surface and bulk treatment conditions", *Vacuum* **47** (6–8), pp. 745–747 (1996).
7B-18. A. van Oostrom and L. Augustus, "Electrical breakdown between stainless-steel electrodes in vacuum", *Vacuum* **32** (3), pp. 127–135 (1982).

Other Articles

Microdischarges over Insulator Surfaces

*7-1. J. P. Vigouroux, C. Le. Gressus, J. P. Duraud, "Electrical surface breakdown: Secondary electron emission and electron spectroscopy of insulators", *Scanning Electron Microscopy/1985/II*, pp. 513–520.
*7-2. C. Biscardi, H. Hseuh, and M. Mapes, "Application of porcelain enamel as an ultra-high-vacuum-compatible electrical insulator", *J. Vac. Sci. Technol. A* **18** (4), pp. 1751–1754 (2000).
*7-3. H. C. Miller and E. J. Furno, "The effect of Mn/Ti surface treatment on voltage-holdoff performance of alumina insulators in vacuum", *J. Appl. Phys.* **49** (11), pp. 5416–5420 (1978).
*7-4. C. Biscardi, H. Hseuh, and M. Mapes, "Application of porcelain enamel as an ultra-high-vacuum-compatible electrical insulator", *J. Vac. Sci. Technol. A* **18** (4), pp. 1751–1754 (2000).
*7-5. S. Michizono, Y. Saito, S. Anami, and A. Kinbara, "Multipactor phenomenon observed at high-power rf windows", *Shinku (J. Vac. Soc. Japan)* **37** (3), pp. 261–263 (1994) (in Japanese).
*7-6. T. Ishii, S. Kobayashi, Tumiran, M. Maeyama, and Y. Saito, "Studies on the changes of alumina surface state by vacuum surface flashover with cathode luminescence spectroscopy", *Shinku (J. Vac. Soc. Japan)* **38** (3), pp. 299–302 (1995) (in Japanese).
*7-7. Tumiran, S. Kobayashi, H. Imada, M. Maeyama, T. Ishii, and Y. Saito, "The measurement of charge distribution on alumina surface after voltage application in vacuum", *Shinku (J. Vac. Soc. Japan)* **38** (3), pp. 307–310 (1995) (in Japanese).
*7-8. H. Kawai, H. Matsuura, S. Michizono, Y. Saito, and A. Inagaki, "Influence of surface treatment on secondary electron emission of alumina ceramics", *Shinku (J. Vac. Soc. Japan)* **36** (3), pp. 256–259 (1993) (in Japanese).
*7-9. S. Michizono, Y. Saito, S. Anami, and A. Kinbara, "Dielectric property of high-power rf window and its breakdown phenomena", *Shinku (J. Vac. Soc. Japan)* **36** (3), pp. 260–262 (1993) (in Japanese).
*7-10. S. Michizono, Y. Saito, T. Sato, and S. Kobayashi, "Surface charging of rf windows", *Shinku (J. Vac. Soc. Japan)* **41** (3), pp. 231–234 (1998) (in Japanese).
*7-11. T. Sugimoto, S. Michizono, Y. Saito, and S. Kobayashi, "Residual stresses of aluminas and their surface flashover voltages in vacuum", *Shinku (J. Vac. Soc. Japan)* **41** (3), pp. 235–238 (1998) (in Japanese).

Microdischarges between High-Voltage Electrodes

*7-12. A. K. Chakrabarti and P. A. Chatterton, "Microparticle trigger discharges and impact damage in a high-voltage vacuum insulated gap", *J. Appl. Phys.* **47** (12), pp. 5320–5328 (1976).

*7-13. S. Kobayashi, Y. Hashimoto, Y. Saito, Y. Yamamoto, and Y. Nagai, "Vacuum breakdown properties of annealed oxygen free copper electrodes", *Shinku (J. Vac. Soc. Japan)* **37** (3), pp. 258–260 (1994).

*7-14. S. Kobayashi, Y. Hashimoto, Y. Saito, Y. Yamamoto, Y. Nagai, K. Takeuchi, and T. Sugano, "Electrical breakdown strength of vacuum gaps between vacuum degassed oxygen-free copper electrodes machined by diamond turning for mirror finish", *Shinku (J. Vac. Soc. Japan)* **37** (3), pp. 289–291 (1994).

*7-15. Y. Hashimoto, S. Kobayashi, Y. Saito, K. Takeuchi, T. Sugano, and Y. Nagai, "Vacuum breakdown properties of vacuum gaps consist of oxygen-free copper electrodes machined by diamond turning for mirror finish", *Shinku (J. Vac. Soc. Japan)* **38** (3), pp. 303–306 (1995).

*7-16. A. Iwai, S. Kobayashi, and Y. Saito, "Charges in copper electrode surface conditions caused by breakdown in ultra-high vacuum", *Shinku (J. Vac. Soc. Japan)* **41** (3), pp. 227–230 (1998).